RSC Advances

PAPER

View Article Online
View Journal | View Issue

Cite this: *RSC Adv.*, 2026, **16**, 23673

Nano-cobalt anchored on chitosan-derived N-doped porous carbon: an efficient catalyst for α-alkylation of ketones with alcohols *via* borrowing hydrogen

Zegang Zhang, Dongbin Mo, Youjuan Tan, Xueqin Chang, Lin Chen * and Xianglin Pei *

Received 1st March 2026
Accepted 30th April 2026

DOI: 10.1039/d6ra01776b

rsc.li/rsc-advances

To address the challenges in developing green and efficient heterogeneous catalysis for the α-alkylation of ketones *via* the borrowing hydrogen strategy, a novel supported cobalt nanoparticle (QNCM@Co) catalyst was rationally designed and prepared. This catalyst features nano-cobalt anchored on N-doped porous carbon microspheres derived from quinoline-8-carboxaldehyde-modified chitosan microspheres. Structural characterization results indicated that the carrier possesses abundant nanopores and N/O functional groups, enabling effective anchoring and uniform dispersion of nano-cobalt particles. Moreover, the Co–N/O coordination structure at the nanoscale surface modulates the electronic structure of the active sites. QNCM@Co exhibited a high catalytic activity in the borrowing hydrogen α-alkylation reaction of ketones and alcohols, which outperformed most reported homogeneous and heterogeneous catalysts. It also demonstrated excellent cycling stability and broad substrate scope.

Introduction

The α-alkylation reaction of ketones with alcohols is a crucial method for constructing C(sp3)–C(sp3) bonds.[1] Particularly in medicinal chemistry, it represents a pivotal tool for the synthesis of commercially relevant bioactive compounds, including nonsteroidal anti-inflammatory drugs (NSAIDs), neuroactive agents, and anticancer therapeutics.[2] However, traditional processes typically rely on haloalkanes as the alkylation reagents, faced with issues such as the need for stoichiometric bases, the generation of toxic waste, and relatively high costs, compromise their long-term sustainability.[3] Alternatively, alcohols can function as inexpensive and green alkylating agents for ketones *via* borrowing hydrogen.[4] In this approach, the alcohol first undergoes dehydrogenation to form an aldehyde, which then condenses with a ketone to produce an α,β-unsaturated ketone. Finally, the extracted hydrogen atoms are transferred back to reduce the *in situ* generated intermediate, achieving the formation of a C(sp3)–C(sp3) bond.[5]

Although noble-metal homogeneous catalysts (such as Ru, Rh, Ir, and Pd) are widely employed in this alkylation reaction with high efficiency, their high cost precludes practical applications.[6] In the pursuit of sustainable chemistry, the development of catalytic systems based on earth-abundant, cost-effective metals (*e.g.*, Co, Fe, Mn, Ni) has emerged as a pivotal research frontier.[7] However, these inexpensive metals suffered from inherently low activity and required expensive N-heterocyclic clamp ligands to maintain efficiency,[8] which hinders their further advances (Fig. 1a). In contrast, heterogeneous catalysts possess significant advantages, such as ease of recovery, reusability, and environmental friendliness, wherein developing cost-effective metal heterogeneous catalytic systems utilizing Co has become a hot topic.[9] Nevertheless, these

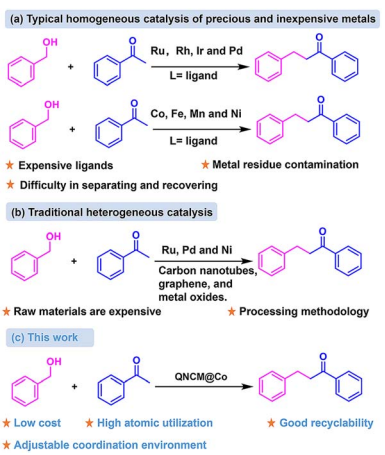

Fig. 1 (a and b) Challenges of the reported catalytic systems for the α-alkylation of ketones with alcohols. (c) Our strategy: the QNCM@Co-empowered α-alkylation of ketones.

School of Chemistry and Materials Science, School of Materials and Architectural Engineering, Guizhou Normal University, Guiyang 550025, China. E-mail: chenlin8310@aliyun.com; xianglinpei@163.com

systems often exhibit high temperatures, high loadings, and a narrow substrate scope.[10] In this context, developing low-cost, readily available, and highly efficient Co heterogeneous catalysts for the α-alkylation of ketones with alcohols is of paramount importance.

The commonly used supports, such as carbon nanotubes, graphene, and metal oxides, are often constrained by expensive raw materials and complex preparation processes (Fig. 1b), which spurs interests in preparing carriers from inexpensive, environmentally friendly, and renewable materials.[11,12] Chitosan, a widely available and low-cost natural polymer derived from chitin, features a well-defined molecular structure rich in easily modifiable amino and hydroxyl groups on the glucosamine unit.[13] The depolymerization and recombination mechanism mediated by intra-chain hydrogen bonds in chitosan effectively governs the morphology of this material.[14] Furthermore, nitrogen-containing heterocycles can be grafted onto chitosan using amino groups as functional handles. These N-heterocycles would serve as coordination sites to immobilize the metal atoms and tailor their electronic structures (Fig. 1c). Therefore, a heterogeneous cobalt catalyst based on a chitosan-derived support, characterized by low dosage, high activity, and excellent stability, is expected to significantly advance the α-alkylation of ketones.

In this work, porous chitosan microspheres (CM) were first prepared *via* the sol–gel method.[15] Quinoline-8-carboxaldehyde was then installed onto their surfaces through the Schiff base reaction (QCM), constructing a multifunctional coordination environment.[16] Finally, the wet impregnation of cobalt followed by the high-temperature *in situ* activation were conducted, resulting in the fabrication of the N-doped porous carbon microsphere supported nano-cobalt (QNCM@Co). The introduction of quinoline structure not only enhanced the carrier stability, but also firmly anchored cobalt nanoparticles. The N and O sites on the carrier modulated the electronic structure of the cobalt nanoparticle surface, thereby significantly boosting the catalytic activity. Employing the borrowing hydrogen strategy, QNCM@Co drove the α-alkylation of ketones with alcohols in high catalytic efficiency, which achieved high TOF values. The catalyst also exhibits a wide range of substrate applications, better activity than commercial catalysts and excellent cycle stability. Thus, a green and sustainable heterogeneous catalytic platform for the current reaction was established. We document here the details of this study.

Experimental section

Preparation of chitosan microspheres

Chitosan powder (9 g) was dissolved in 200 g of an aqueous solution comprising LiOH (9 wt%), KOH (14 wt%), and urea (16 wt%). The solution was frozen at −35 °C for 3–4 h and subsequently thawed under stirring at room temperature. This freeze-thaw cycle was repeated three times to afford a clear and transparent chitosan solution. Subsequently, 350 g of isooctane and 20 g of Span 85 were added to a 1 L three-neck flask equipped with a mechanical stirrer. After 0.5 h of stirring in an ice bath, the chitosan solution was added dropwise. The mixture was stirred continuously in an ice-water bath for 1 h to form uniform emulsion droplets. The mixture was then transferred to a 70 °C water bath and stirred for 30 min. Upon completion, the suspension was filtered, and the filter cake was washed sequentially with ethanol and deionized water. Finally, freeze-drying of the filter cake afforded the porous chitosan microspheres (CM).

Preparation of CM grafted by quinoline-8-carboxaldehyde

A mixture of CM (500 mg) and quinoline-8-carboxaldehyde (332 mg) was added to a 200 mL double-stoppered round-bottom flask. Anhydrous ethanol (50 mL) was added, and the pH of the solution was adjusted to 6 with acetic acid. The mixture was then refluxed at 80 °C for 12 h. After the reaction was complete, the mixture was filtered. The filter cake was washed three times with ethanol, and subsequently with tert-butanol. Freeze-drying of the resulting solid afforded quinoline-8-carboxaldehyde-grafted chitosan microspheres (QCM).

Preparation of QNCM@Co

QCM (500 mg) was dispersed in 100 mL of ethanol and stirred at room temperature for 5–10 min. Separately, CoCl2·6H2O (60.5 mg) was dissolved in 20 mL of ethanol. Upon the formation of a clear solution, it was added dropwise to the QCM dispersion. The mixture was continuously stirred at room temperature for 3 h. After that, the solid was collected by filtration and washed repeatedly with ethanol and deionized water to afford the precursor. Subsequently, the precursor was calcined under an argon atmosphere at a heating rate of 5 °C min^{-1} to 600 °C, and maintained at this temperature for 2 h. After cooling, QNCM@Co was obtained. With commercial carbon powder as a support, a carbon-supported nano-cobalt (C@Co) was prepared under the same procedure. The carrier was replaced with CM, and CM@Co was prepared using the same procedure.

General procedure for the α-alkylation of ketones with alcohols

In a flask equipped with a magnetic stirrer, ketone (0.2 mmol), alcohol (0.4 mmol), NaOH (8.0 mg, 0.2 mmol), and QNCM@Co (1.0 mg, 0.23 mol% of Co loading) were sequentially added, followed by the addition of toluene (2 mL). The mixture was stirred at 130 °C for 24 h. After completion, the coupling reaction product was analyzed by gas chromatography (GC) and ^{1}H NMR spectroscopy, with biphenyl as an internal standard.

Result and discussion

Preparation and characterization

The preparation process of the N-doped porous carbon microsphere nano-cobalt catalyst is shown in Fig. 2a. Chitosan powder was dissolved in a cold alkali/urea aqueous solution, and the hydrogen bonds between and within the molecules were destroyed, resulting in the formation of a transparent solution.[17] Using the microemulsion-assisted sol–gel method, the dissolution equilibrium was disrupted by rapid stirring to facilitate the reorganization of chitosan chains through

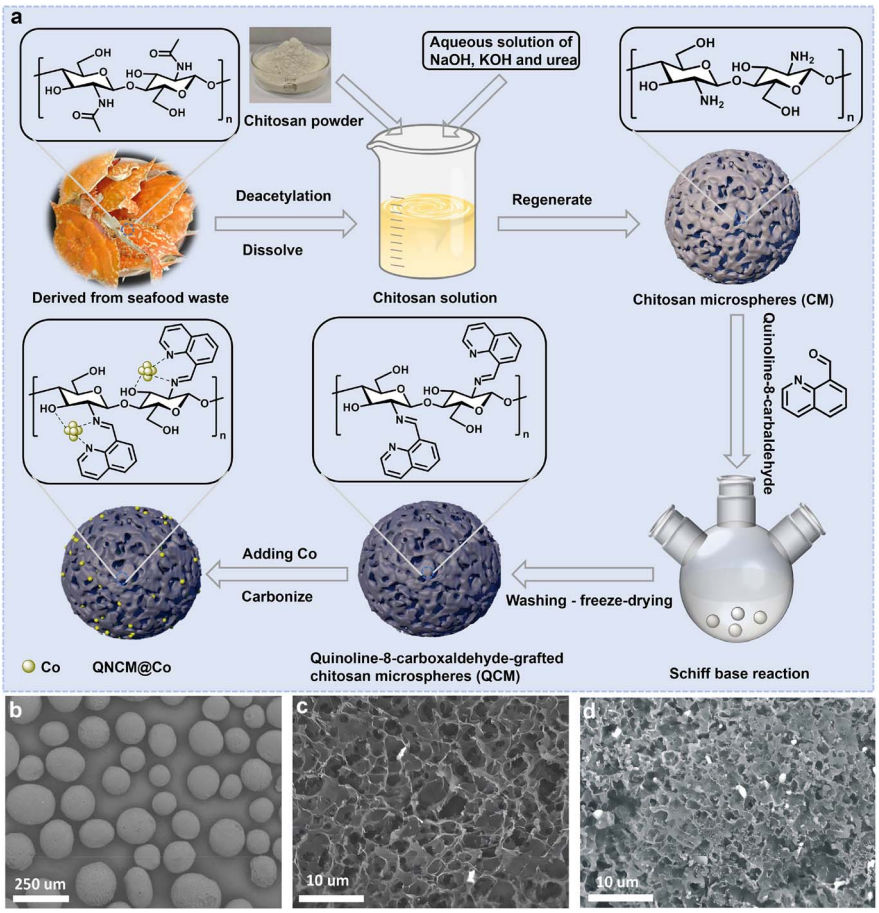

Fig. 2 (a) Schematic diagram of the preparation process of QNCM@Co. (b–d) SEM images of QNCM@Co.

hydrogen bonding, resulting in the formation of three-dimensional porous CM. Leveraging the abundant amino groups on the surface of CM, quinoline-8-carboxaldehyde was installed onto the microsphere surface *via* a Schiff base reaction, which furnished quinoline-8-carboxaldehyde grafted chitosan microspheres (QCM) with N/O coordination sites. Cobalt was anchored on QCM *via* wet impregnation using CoCl2·6H2O as the precursor. To achieve the *in situ* growth of nano-cobalt, the material was calcined under an argon atmosphere at high-temperature, causing the fabrication of the N-doped porous carbon microsphere-supported nano-cobalt (QNCM@Co). This procedure can increase the specific surface area and pore density of the catalyst, thus enhancing mass transfer efficiency. The abundant N/O coordination sites effectively anchored cobalt nanoparticles, preventing their aggregation at high temperatures. Furthermore, they can modulate the electronic structure of the cobalt nanoparticle surface, thereby potentially boosting the catalytic performance.

A series of characterizations was conducted to investigate the structural properties of QNCM@Co. In the scanning electron microscopy (SEM) images, QNCM@Co exhibited three-dimensional nanoporous structures (Fig. 2b–d), which guaranteed the uniform decoration of quinoline on the microsphere surface.

Nitrogen adsorption–desorption testing (Fig. 3a) manifested that both N-doped porous carbon microspheres (QNCM) and QNCM@Co displayed Type IV isotherms and H3-type hysteresis loops, confirming the presence of mesoporous structures in the material.[18] Their pore size distribution primarily ranged from 0 to 60 nm, with a main pore size of approximately 8 nm (Fig. 3b). Additionally, the specific surface area of QNCM@Co was 175.16 m2/g, lower than that of the blank support (205.07 m2/g), which was attributed to the formation of nano-cobalt particles occupying part of pore structures. This high specific surface area not only provided more anchor points for nano-scale cobalt, but also improved mass transfer efficiency in the reaction.

In the FT-IR spectra (Fig. 3c), CM, QCM, and QNCM@Co showed hydroxyl (O–H) stretching vibration peaks at 3435 cm^{-1}, amide N–H (–CO–NH–) bending peaks at 1594 cm^{-1}, and ether bond (C–O–C) vibration at 1354 cm^{-1}.[19] Compared to CM, QCM and QNCM@Co exhibited distinct absorption peaks at 1640 cm^{-1} for the C=N bond,[20] along with the C=C vibration peaks at 1450 cm^{-1} to 1600 cm^{-1},[21] suggesting the successful grafting of quinoline-8-carbaldehyde onto the microsphere *via* imine bond.

The X-ray diffraction (XRD) patterns of QNCM and QNCM@Co are depicted in Fig. 3d. Characteristic diffraction

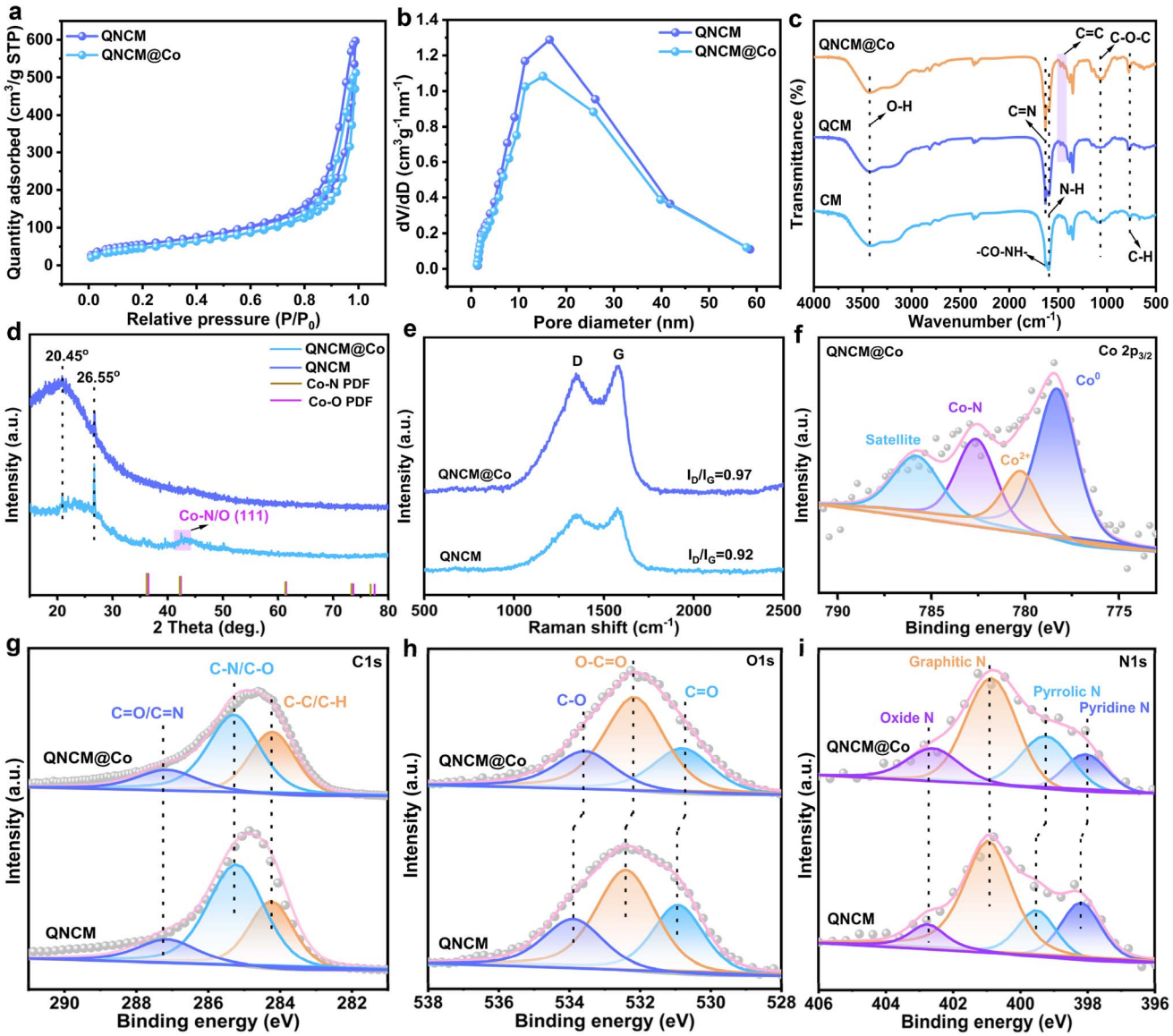

Fig. 3 (a) Nitrogen adsorption/desorption isotherms of QNCM and QNCM@Co. (b) Pore size distribution diagrams of QNCM and QNCM@Co. (c) FT-IR spectra of CM, QCM and QNCM@Co. (d) XRD spectra of QNCM and QNCM@Co, with the standard XRD cards for Co–N and Co–O. (e) Raman spectra of QNCM and QNCM@Co. (f) XPS spectra of Co 2p3/2 for QNCM@Co. (g) C 1s, (h) O 1s, (i) N 1s spectra of QNCM and QNCM@Co.

peaks of chitosan were observed at 20.86° and 26.66° for the both samples, indicating that the structure of the carrier remained stable after grafting.[22] After the support was loaded with cobalt, new characteristic diffraction peaks appeared at approximately 42.67°, corresponding to the (111) crystal planes of Co–N/O, respectively.[23] Comparison with the standard reference pattern (JCPDS card) revealed that these peaks are attributed to nano-cobalt particles with a Co–N/O coordination structure, thereby indirectly confirming the successful doping of quinoline nitrogen.

The Raman spectra of QNCM and QNCM@Co (Fig. 3e) showed two characteristic peaks at ~1343.93 and ~1580.46 cm^{-1}, assigned to the D and G bands of the carbon material, respectively.[24] The D band reflects structural defects in carbon materials, while the G band is associated with the planar stretching motion of sp2 carbon atoms. The graphitization degree and structural order of a material can be evaluated through the intensity ratio of the D band to the G band (ID/IG). The results indicated that the ID/IG ratio of the QNCM@Co slightly increased, suggesting that the introduction of nano-scale cobalt not only improved the graphitization degree of the material, but also led to the formation of more structural defects. Enhanced graphitization improves electrical conductivity, while abundant defect sites facilitate stronger anchoring of metal nanoparticles, collectively boosting catalytic performance.

The chemical state of the QNCM@Co was analyzed by X-ray photoelectron spectroscopy (XPS), and the C 1s spectrum was corrected at 284.80 eV. The full-size XPS spectrum confirmed the presence of C, O, N, and Co elements in QNCM@Co

(Fig. S1). Four peaks at 778.34 eV, 780.24 eV, 782.64 eV, and 785.84 eV appeared in the Co 2p3/2 spectrum, which belonged to Co^0, Co^{2+}, Co–N, and a satellite peak of Co^{2+},[25] respectively (Fig. 3f). The first peak at 778.34 eV indicated that metallic Co was formed *in situ* during pyrolysis. The peak at 780.24 eV may resulted from interactions between N and O elements and cobalt nanoparticles, where the cobalt nanoparticles transferred electrons to the N and O elements, leading to the accumulation of partial positive charge on the surface of the cobalt nanoparticles. The peak at 782.64 eV was assigned to Co–N, verifying the presence of Co–N species in QNCM@Co. This finding corroborated the (111) and (200) crystal planes of Co–N/O observed in the XRD pattern. Compared to QNCM, the C1s spectrum (Fig. 3g) of QNCM@Co could be resolved into C–C/C–H (284.82 eV), C–O/C–N (285.25 eV), and C=O/C=N (287.30 eV) peaks.[26] These C 1s spectral peaks remained essentially unchanged after the introduction of cobalt, and it implied that the carbon elements in the carrier did not interact with the nano-cobalt. In contrast, C=O (530.85 eV), O–C=O (532.15 eV), and C–O (533.65 eV) in the O1s spectrum of QNCM@Co shifted toward lower binding energies compared to C=O (531.02 eV), O–C=O (532.51 eV), and C–O (534.02 eV) in that of QNCM (Fig. 3h).[27] In the N 1s spectra (Fig. 3i), they can be resolved into four peaks assigned to pyridine nitrogen, pyrrole nitrogen, graphitic nitrogen, and oxidized nitrogen, respectively. It is noteworthy that the binding energies of graphitic nitrogen (400.97 eV) and oxidized nitrogen (402.85 eV) did not shift. However, the binding energies of pyridinic nitrogen (398.17 eV) and pyrrolic nitrogen (399.57 eV) shifted to lower binding energies, reaching 397.95 eV and 399.05 eV for QNCM@Co, respectively.[28] This indicated significant interactions between the cobalt nanoparticles and the N and O elements in the support. Due to the high electronegativity of N and O, electron transfer occurred from the cobalt nanoparticles to N and O. This result confirmed that N and O in the carrier form Co–N/O coordination species. These species not only prevent their agglomeration, but also regulated the electronic structure on the nano-cobalt surface, thereby enhancing its ability for the activation of substrates.

Transmission electron microscopy (TEM) analysis was performed to unveil the morphological features of the nano-cobalt. It was shown that C@Co exhibited obvious sintering phenomenon for cobalt (Fig. 4a and b), while cobalt nanoparticles of QNCM@Co were uniformly distributed on the surface of N-doped porous carbon microspheres (Fig. 4c). This striking contrast provided clear evidence of the anchoring effect of N/O species on cobalt nanoparticles. HRTEM analysis revealed distinct lattice fringes in cobalt nanoparticles with an interplanar spacing of 0.242 nm (Fig. 4d–f), verifying the successful loading of cobalt onto the QCM carrier while exhibiting a uniform dispersion.[29] This is primarily attributed to the strong coordination of N (quinoline and imine) and O (hydroxyl group) toward cobalt, while the nanoporous structure of CM also facilitated the stable dispersion of cobalt nanoparticles.

Catalytic performance of QNCM@Co in the α-alkylation of ketones with alcohols

The QNCM@Co-mediated α-alkylation reaction of acetophenone **1a** with benzyl alcohol **2a** was conducted to evaluate its catalytic ability. The effects of solvents, bases, substrate stoichiometry, and temperature on the reaction outcomes were assessed. Solvents with different polarities were screened (Fig. 5a). It was found that toluene was the better choice among the commonly used solvents, and the reaction generated product **3a** with a yield of 27%. Various organic and inorganic bases were evaluated to enhance the reaction efficiency (Fig. 5b). The reaction using NaOH afforded the product in an 85% yield, significantly higher than that obtained with other bases. Subsequently, the influence of alkali loading on the reaction was examined (Fig. 5c). However, any deviation from the optimal NaOH dosage led to a reduction in product yield, which might be attributed to sluggish reaction kinetics (0.1 mmol) or over-reduction of the product (0.3 mmol and 0.4 mmol). The optimal molar ratio of **1a** to **2a** was determined to be 1 : 2 (Fig. 5d). In addition, temperature screening showed that the highest yield (98%) was achieved at 130 °C after 24 h (Fig. 5e). When the temperature raised to 140 °C, the yield of the target product decreased significantly, due to excessive reduction of the target product in the high temperature. Without a catalyst, the reaction yield was only 19%. Interestingly, the carrier itself (QNCM) was capable of driving the reaction, affording the product in 32% yield. This observation suggested that the carrier possesses abundant nitrogen sites capable of binding to alkali metals, thereby facilitating the reaction progression.

The QNCM@Co was compared with various cobalt catalysts,[30] including C@Co, commercially available nano-cobalt, cobalt oxide, homogeneous cobalt chloride, and CM@Co (Fig. 5f). The catalytic activity of C@Co was significantly lower than that of QNCM@Co, and it indicated that N/O can modulate the electron structure of cobalt, thereby enhancing catalytic activity. The rest of catalysts also achieved inferior yields, which indirectly corroborated the above inference. After the reaction was complete, we performed GC-MS analysis on the reaction mixture for each catalyst to evaluate the chemoselectivity (Fig. S2). Only target product (1,3-diphenyl-1-propanone **3a**) was detected for QNCM@Co, whereas, for the other catalysts, the target product together with many by products, consisting of unreacted chalcone, over-reduced 1,3-diphenylpropan-1-ol, and 3-benzyl-1,5-diphenylpentan-1,5-dione, were detected. Therefore, QNCM@Co exhibited the best catalytic activity and selectivity among others. QNCM@Co also displayed superior catalytic activity compared to some reported heterogeneous and homogeneous catalysts (Table S2). Furthermore, it demonstrated a superior TOF of 17.75 h^{-1} (Fig. 5g) and excellent substrate compatibility under mild conditions with low catalyst dosage, highlighting the successful synthesis *via* a green and efficient route.[31]

The stability of the QNCM@Co catalyst was assessed by conducting cyclic tests using the model reaction under the optimal conditions. Following each reaction, the catalyst was

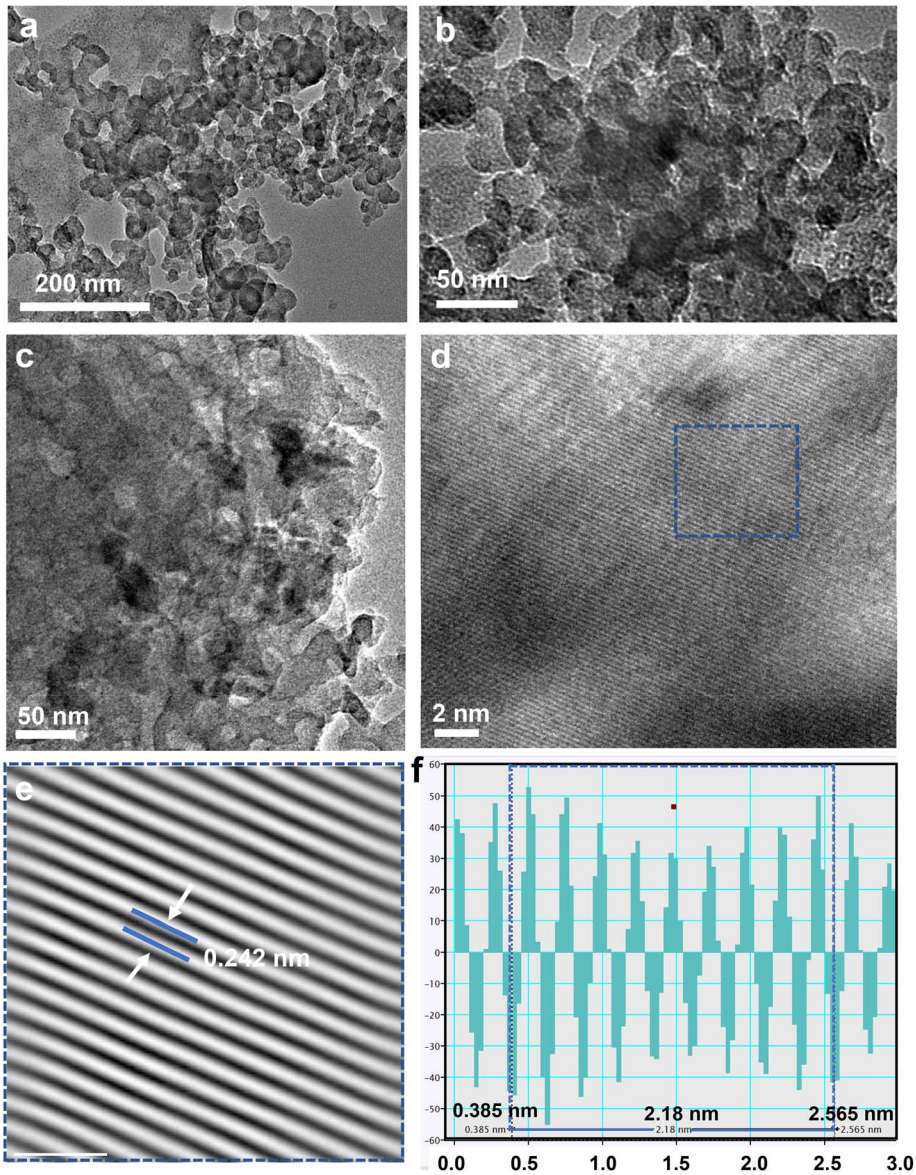

Fig. 4 (a) and (b) TEM images of particle size distributions of C@Co. (c) TEM and (d) HRTEM images of particle size distributions of QNCM@Co. (e) Enlarged view of the blue box in Fig. (d): the crystal lattice striations of QNCM@Co. (f) Calculation for the lattice spacing of QNCM@Co.

retrieved *via* centrifugation, washed, and dried before being directly employed in the next cycle. As depicted in Fig. 5h, the catalyst maintained 90% yield of the target product (**3a**) after five cycles, exhibiting no appreciable degradation in activity. Inductively coupled plasma optical emission spectroscopy (ICP-OES) showed a marginal decrease in cobalt loading from 3.49% to 3.28% (Fig. 5i), confirming that cobalt leaching was negligible. These data substantiate the superior stability of QNCM@Co and highlight the pivotal role of the N and O-containing functional groups in the support for anchoring and regulating the nanoscale cobalt particles.

The substrate scope of the QNCM@Co-catalyzed α-alkylation of ketones with alcohols was carefully examined (Table 1). Various aryl ethanones (**1b–i**, R1) first reacted with benzyl alcohol **2a** for the evaluation. When electron-donating groups (**1b:** $-CH_3$ and **1c:** $-OCH_3$) or electron-withdrawing groups (**1d:** –Cl and **1e:** –I) were attached to the *para*-position of the phenyl ring in acetophenone, the reaction still proceeded with comparable efficiency, giving rise to the generation of products **3b–e** in 86–92% yields. The *meta*-substitution (**1f**) and di-substitution (**1g**) were also tolerated, as shown by the synthesis of the corresponding products (**3f** and **3g**). Both 2-naphthylethanone (**1h**) and 1-(quinolin-6-yl)ethanone (**1i**) worked well in the reaction, and good results were obtained (**3h** and **3i**). Subsequently, we turned to focus on the compatibility of the catalytic system towards a series of aryl methanols (**2b–j**, R2). The protocol could accommodate the substituted benzyl alcohols (**2b–h**), regardless of position (*para*, *meta* and 3,5-di-substitution), electronic nature (–CH3, –OCH3, –F, and –Br) and steric hindrance (*ortho*) of the substituents on the phenyl ring,

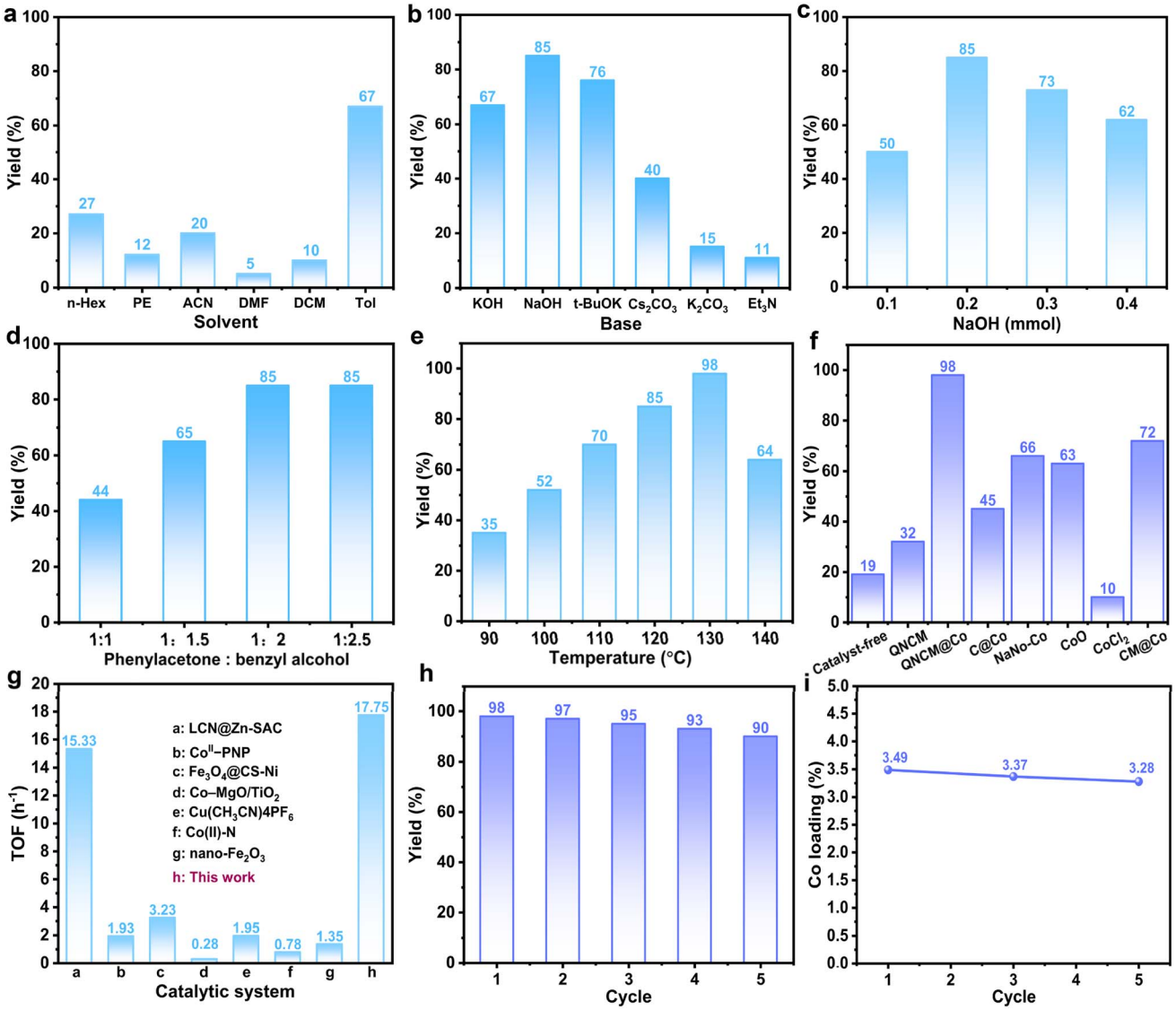

Fig. 5 Reaction conditions unless noted: **1a** (0.2 mmol), **2a** (0.4 mmol, 2.0 equiv.), catalyst (0.23 mol% of Co) and base (0.2 mmol, 1.0 equiv.) in solvent (2 mL); yield was determined by gas chromatography using diphenyl as an internal standard. The effects of (a) solvent, (b) base, (c) the amount of NaOH, (d) the molar ratio of substrates, and (e) temperature on the reaction. (f) Comparative studies on the activities of different cobalt catalysts. (g) Comparisons of TOF between QNCM@Co and some reported heterogeneous or homogeneous catalysts. (h) Recycling activity of QNCM@Co. (i) ICP-OES data of the QNCM@Co in 5 runs.

and products **3j–p** were gained in 81–91% yields. The presence of fused-aromatic (**2i**) and heteroaromatic (**2j**) moieties did not compromise the reaction efficiency, as high yields were still achieved (**3q**: 90% and **3r**: 82%).

Mechanism studies

It is generally accepted that in the presence of a base, QNCM@Co first promotes the dehydrogenation of benzyl alcohol **2a** to deliver benzaldehyde, while simultaneously transferring the α-H of **2a** to the metal center, leading to the formation of a metal hydride (M–H). Subsequently, benzaldehyde undergoes an aldol reaction with acetophenone **1a** followed by dehydration elimination to give a chalcone intermediate. Finally, the C=C moiety of this intermediate is selectively reduced by M–H to afford the target product 1,3-diphenylpropane-1-one **3a**,[32] while completing the catalytic cycle (Fig. 6d). To validate this reaction pathway, the reaction mixture was detected by gas chromatography GC at 3 h, 6 h, 9 h, 12 h, and 15 h, with results shown in Fig. 6a. As the reaction proceeded, the chromatographic peak for benzyl alcohol gradually decreased while that for benzaldehyde appeared, indicating the successful oxidation of benzyl alcohol. Concurrently, the peak corresponding to the chalcone intermediate gradually weakened, while the signal for the target product, 1,3-diphenylpropane-1-one, progressively intensified. Gas chromatography data revealed that the reaction process includes dehydrogenation of alcohols, condensation, and hydrogenation

Table 1 Substrate scope for the QNCM@Co-catalyzed α-alkylation of ketones with alcohols[a]

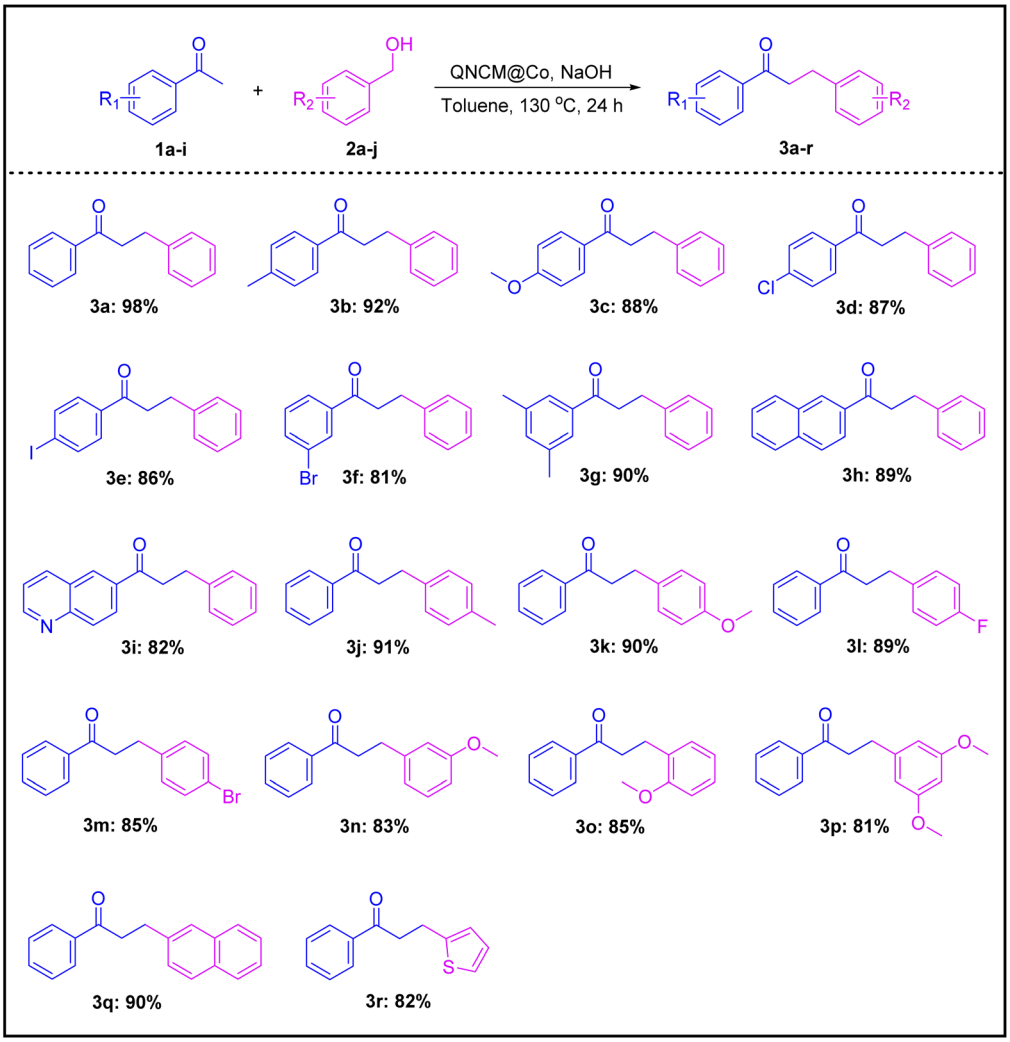

[a] Reaction conditions: **1** (0.2 mmol), **2** (0.4 mmol, 2 equiv.), QNCM@Co (1.0 mg, 0.23 mol% of Co) and NaOH (8.0 mg, 0.2 mmol, 1.0 equiv.) in toluene (2 mL). [b]Yield was determined by ^{1}H NMR after the product was purified on silica gel column.

of chalcones, consistent with the conventional hydrogen borrowing pathway.

The rate-determining step (RDS)[33] was confirmed by kinetic experimental analysis (Fig. 6b). The results revealed that the rate constant for the overall reaction between acetophenone and benzyl alcohol ($k_1 = 0.21$) was significantly lower than that for the reaction between chalcone and benzyl alcohol ($k_2 = 0.76$). Given that the condensation step proceeds spontaneously, the oxidation of benzyl alcohol to benzaldehyde is identified as the RDS for the reaction. To further clarify the origin of hydrogen during hydrogen borrowing, the overall reaction was decomposed into three steps (Fig. 6c): In Reaction 1, benzyl alcohol reacted with QNCM@Co to afford benzaldehyde in a 14% yield, confirming the ability of the catalyst to facilitate alcohol dehydrogenation and the formation of the metal hydride species. The low yield might attribute to the absence of a hydrogen acceptor. In Reaction 2, benzaldehyde and acetophenone were stirred together for 24 h, but the target product 1,3-diphenylpropane-1-one was not detected; instead, chalcone was gained in a 99% yield. This observation indicated that without alcohol, the system lacks a hydrogen source and is unable to reduce chalcone to the target product. In Reaction 3, chalcone reacted with benzyl alcohol in the presence of QNCM@Co to furnish the target product in a 99% yield, demonstrating that the reduction of chalcone is achieved *via* hydrogen transfer from benzyl alcohol. Collectively, the gas chromatography monitoring data and stepwise experimental results validated the proposed hydrogen transfer mechanism between acetophenone and benzyl alcohol, which matches the catalytic cycle depicted in Fig. 6d.

DFT calculations

Based on characterization results from XPS, FT-IR, and other tests, two catalyst models were established: C@Co without N/O

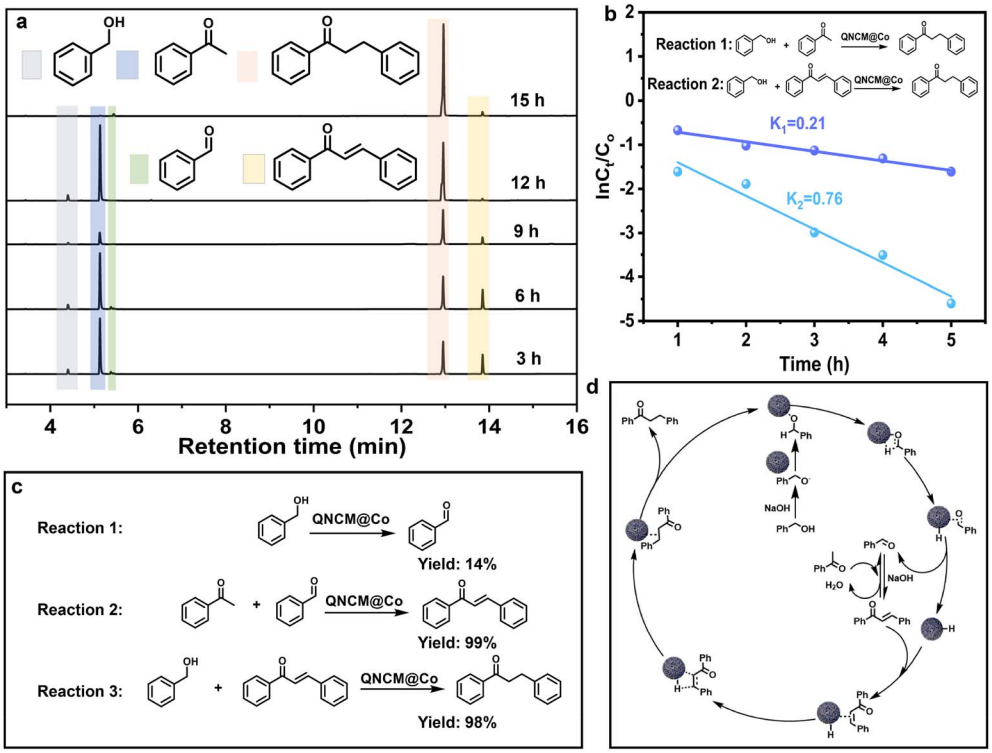

Fig. 6 (a) GC spectra over time for the α-alkylation reaction of acetophenone **1a** with benzyl alcohol **2a** catalyzed by QNCM@Co. (b) Kinetic curves; C_0: the initial concentration of substrate; C_t: substrate concentration at time t; K: rate constant. (c) Stepwise experiments for the reaction. (d) Proposed reaction mechanism.

and QNCM@Co doped with N/O. By calculating the formation energies and Bader charges of both materials, the effects of N/O doping on the structural stability and electronic properties of the catalysts were unveiled, and their roles in the reaction mechanism of the current α-alkylation were elucidated. It was shown that the formation energy of C@Co (−2.45 eV, Fig. 7a) is much higher than that of QNCM@Co (−4.87 eV, Fig. 7b), which indicated that N/O doping facilitates the decrease of the formation energy barrier for the cobalt nanostructure, thereby enhancing the structural stability of the catalyst. Further Bader charge analysis, where yellow and blue represent electron enrichment and depletion, respectively (Fig. 7c and d), showed that QNCM@Co features a charge transfer of 0.97 e from the cobalt nanoparticle surface to the support, which is higher than 0.94 e observed for C@Co. These results revealed that N/O doping makes the cobalt nanoparticle surface of QNCM@Co more electron-deficient. In the current hydrogen-transfer α-alkylation reaction, the benzoyl anion, formed by deprotonation, exhibits electron-rich characteristics. Consequently, it is easier to be adsorbed onto the electron-deficient cobalt nanoparticle surface. This nature lowers the energy barrier for the RDS—the oxidation of benzyl alcohol to benzaldehyde—thereby accelerating the entire catalytic cycle.

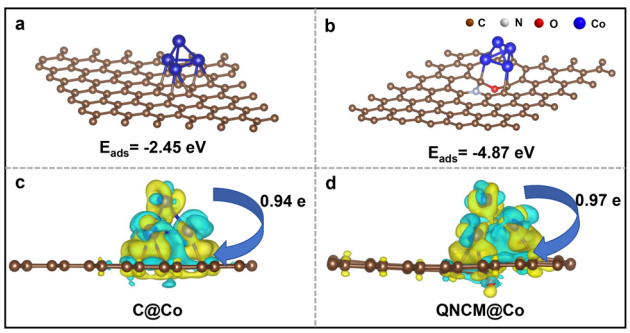

Fig. 7 (a) The formation energy of C@Co and (b) the formation energy of QNCM@Co. (c) The Bader charge of C@Co and (d) the Bader charge of QNCM@Co.

Conclusion

In summary, this study employed cost-effective and abundant chitosan as the raw material to prepare CM. Harnessing the Schiff base reaction, quinoline-8-carboxaldehyde was grafted onto its surface (QCM), followed by the wet impregnation of cobalt and the high-temperature activation to fabricate QNCM@Co. The structure–performance relationship of QNCM@Co was then systematically investigated. The results demonstrated that this N-doped material possesses two key advantages: first, the nitrogen atoms of quinoline and imine form stable bidentate coordination with cobalt, effectively anchoring Co nanoparticles during activation, promoting their uniform dispersion, and inducing the formation of Co–N/O coordination species. This optimizes the cobalt coordination environment and electronic structure, thereby enhancing

intrinsic activity. Second, the large specific surface area and abundant pore structure of the carrier facilitate reactant diffusion and product adsorption/desorption, accelerating mass transfer and improving catalytic efficiency. Compared to various commercially available cobalt catalysts, QNCM@Co exhibited outstanding activity in the α-alkylation of ketones with alcohols. Furthermore, benchmarked against state-of-the-art homogeneous and heterogeneous systems, along with excellent cycling stability and substrate compatibility. These findings underscored the potential of the QNCM@Co catalyst for the green synthesis of α-alkylated compounds.

Author contributions

Zegang Zhang: conceptualization, writing – review & editing, visualization, formal analysis, investigation, data curation. Dongbin Mo, Youjuan Tan and Xueqin Chang: formal analysis, investigation, data curation. Lin Chen and Xianglin Pei: conceptualization, writing – review & editing, visualization, formal analysis, investigation, data curation.

Conflicts of interest

There are no conflicts to declare.

Data availability

The datasets generated during and/or analyzed during the current study are available from the corresponding author on reasonable request.

Supplementary information (SI) is available. See DOI: https://doi.org/10.1039/d6ra01776b.

Acknowledgements

This work was supported by the Key Project of Natural Science Foundation of Guizhou Province (No. ZK [2023] Key 025 and No. ZD [2026] 107), the Guizhou Province Science and Technology Project (Qian Ke He Ji Chu MS [2026] 426 and No. [2024] Normal 072), the Qiannan Normal College for Nationalities University Science Park (No. ZZSG [2024] 002), the Project of Scientist Workstation (No. KXJZ [2024] 028), the Lightweight Materials Engineering Research Center of the Education Department of Guizhou (No. [2022] 045), and the National Natural Science Foundation of China (21762013).

References

1 E. Suarsih, Y. Kita, K. Kamata and M. Hara, *Catal. Sci. Technol.*, 2022, **12**, 4113–4117.
2 D. Bhattacharyya, P. Adhikari, N. Hazarika, B. K. Sarmah and A. Das, *ChemCatChem*, 2023, **15**, e202300542.
3 D. Y. Yang, H. L. Wang, C. Liu and C.-R. Chang, *Catal. Sci. Technol.*, 2023, **13**, 3174–3181.
4 F. Freitag, T. Irrgang and R. Kempe, *Chem. Eur J.*, 2017, **23**, 12110–12113.
5 G. Q. Zhang, J. Wu, H. S. Zeng, S. Zhang, Z. W. Yin and S. P. Zheng, *Org. Lett.*, 2017, **19**, 1080–1083.
6 L. Rakers, F. Schäfers and F. Glorius, *Chem. Eur J.*, 2018, **24**, 15529–15532.
7 M.-S. Abdallah, N. Joly, S. Gaillard, A. Poater and J.-L. Renaud, *Org. Lett.*, 2022, **24**, 5584–5589.
8 J. Das, K. Singh, M. Vellakkaran and D. Banerjee, *Org. Lett.*, 2018, **20**, 5587–5591.
9 M. Taheri-Torbati and H. Eshghi, *Appl. Organomet. Chem.*, 2022, **36**, 574–583.
10 X. P. Zhang, G.-P. Lu, K. Wang, Y. M. Lin, P. C. Wang and W. B. Yi, *Nano Res.*, 2021, **15**, 1874–1881.
11 A. E. F. Denjean, A. Nova and D. Balcells, *ACS Catal.*, 2024, **14**, 11332–11342.
12 M. K. Kajal and H. P. Nayek, *Dalton Trans.*, 2025, **54**, 13326–13336.
13 T. J. Madera-Santana, C. H. Herrera-Méndez and J. R. Rodríguez-Núñez, *Green Mater.*, 2018, **6**, 131–142.
14 X. L. Zheng, Y. Li, W. D. Li, X. L. Pei and D. D. Ye, *Int. J. Biol. Macromol.*, 2023, **241**, 124615.
15 X. G. Yin, Q. D. Zhu, Y. J. Tan, S. Long, Y. Huang, Y. Li and X. L. Pei, *Appl. Surf. Sci.*, 2024, **648**, 159047.
16 J. P. Kujur, P. R. Moon and D. D. Pathak, *Int. J. Biol. Macromol.*, 2023, **252**, 126497.
17 Q. P. Li, J. Sun, L. H. Zhuang, X. Q. Xu, Y. Sun and G. W. Wang, *Carbohydr. Polym.*, 2018, **195**, 288–297.
18 J. Y. Zhang, F. L. Zhu, Y. Zhang, M. Y. Zhu, H. L. Li and B. Dai, *Korean J. Chem. Eng.*, 2022, **39**, 1768–1774.
19 Q. D. Zhu, X. G. Yin, Y. J. Tan, D. D. Wei, Y. Li and X. L. Pei, *Int. J. Biol. Macromol.*, 2024, **254**, 127949.
20 M. Sajjadi, M. Nasrollahzadeh, H. Ghafuri, T. Baran, Y. Orooji, N. Y. Baran and M. Shokouhimehr, *Int. J. Biol. Macromol.*, 2022, **209**, 1573–1585.
21 W. Wang, Z. F. Xiao, C. F. Huang, K. W. Zheng, Y. Luo, Y. M. Dong, Z. T. Shen, W. Li and C. Q. Qin, *Polymers*, 2019, **11**, 1417.
22 Q. Jin, Y. D. Li, D. S. Yang and J. H. Cui, *RSC Adv.*, 2018, **8**, 1255–1264.
23 X. Han, S. Y. He, J. F. Sun, J. W. Mu, S. W. Chen, J.-C. Ren, Y. G. Yu, C.-J. Jia and R. Si, *ACS Catal.*, 2025, **15**, 20796–20806.
24 C. L. Yang, L. Luo, T. X. Zhao, J. X. Cao and Q. Lin, *Chem. Eng. J.*, 2025, **512**, 162597.
25 D. Liu, P. Yang, H. Zhang, M. J. Liu, W. F. Zhang, D. M. Xu and J. Gao, *Green Chem.*, 2019, **21**, 2129–2137.
26 J. P. Zhou, X. L. Yang, Q. P. Wei, Y. Q. Lan and J. Guo, *J. Environ. Manage.*, 2023, **327**, 116895.
27 G. S. Wang, Z. Hu, Z. P. Chen, J. W. Wang, J. S. Hu and X. X. Xu, *Appl. Surf. Sci.*, 2023, **631**, 157538.
28 Y. X. Zhu, Q. D. Zhu, Y. J. Tan, H. Q. Wang, X. F. Liu, W. Gong, D. D. Ye and X. L. Pei, *Green Chem.*, 2025, **27**, 6607–6618.
29 W. Li, R. Meng, K. C. Wang, Y. J. Cheng, D. G. Cai and G. W. Zhan, *Appl. Catal. B Environ. Energy*, 2025, **365**, 124906.
30 L. N. Zhang, D. H. Yao, X. Wang and D. Zhang, *Asian J. Org. Chem.*, 2024, **13**, e202400350.

31 A. Cook and S. G. Newman, *Chem. Rev.*, 2024, **124**, 6078–6144.
32 A. Mandal, M. Pradhan, C. Mitra, S. Nandi, B. Sadhu and S. Kundu, *ACS Catal.*, 2024, **15**, 706–718.
33 Y. Kita, M. Kuwabara, K. Kamata and M. Hara, *ACS Catal.*, 2022, **12**, 11767–11775.